Original

Nene, S.S.; Estrin, Y.; Kashyap, B.P.; Prabhu, N.; Al-Samman, T.; Luthringer, B.J.C.; Willumeit, R.:

Towards microstructure-cytocompatibility relationship in ultralight Mg-4Li-1Ca (LX41) alloy for degradable implant applications.

In: BioNanoMaterials. Vol. 17 (2016) 3-4, 103 - 111.
First published online by de Gruyter: 25.02.2016

http://dx.doi.org/10.1515/bnm-2015-0019

Saurabh Sanjay Nene, Yuri Estrin*, Bhagawati Prasad Kashyap, Nithyananad Prabhu, Talal Al-Samman, Berengere J.C. Luthringer and Regine Willumeit

Towards microstructure-cytocompatibility relationship in ultralight Mg-4Li-1Ca (LX41) alloy for degradable implant applications

DOI 10.1515/bnm-2015-0019
Received November 6, 2015; accepted February 2, 2016

Abstract: Cytocompatibility and biodegradation behaviour were investigated for a newly developed ultralight Mg-4Li-1Ca (LX41) alloy with different starting microstructures. This established the important role of microstructure in determining the pH variation, H_2 evolution and amount of ions (Mg, Li, Ca) released during degradation. Thus, different thermomechanical treatments were utilised to alter the microstructure of the alloy and to evaluate its bio-response. The as-cast and two step rolled+annealed (TA30) materials showed stronger X-ray diffraction peaks for Mg- and Li-containing hydroxyapatite (HA) than the two step rolled (TSR) and the equal channel angular pressed (ECAP) materials. It was also found that the as-cast and TA30 variants of LX41 showed good cell viability of more than 100% with preferential attachment and healthier cell morphology than the TSR material. This is associated with greater content of Mg and Li ions released during alloy degradation. These act as mediators to establish contact between the cells and the substrate, and thereby promote cell attachment and proliferation. These findings suggest the existence of a strong microstructure-cytocompatibility relation for the present LX41 alloy, which can be used as an important tool for further magnesium alloy development for biological applications.

Keywords: biodegradable implants; cytocompatibility; hydroxyapatite; LX41 alloy; microstructure.

***Corresponding author: Yuri Estrin,** IITB-Monash Research Academy, Powai, Mumbai 400076, India; Department of Materials Science and Engineering, Monash University, Clayton, Victoria 3800, Australia; and Laboratory of Hybrid Nanostructured Materials, Moscow Institute of Steel and Alloys, Leninsky prosp. 4, Moscow 119049, Russia, e-mail: yuri.estrin@monash.edu
Saurabh Sanjay Nene: IITB-Monash Research Academy, Powai, Mumbai 400076, India; Department of Materials Science and Engineering, Monash University, Clayton, Victoria 3800, Australia; and Indian Institute of Technology Bombay, Department of Metallurgical Engineering and Materials Science, Powai, Mumbai 400076, India
Bhagawati Prasad Kashyap and Nithyananad Prabhu: IITB-Monash Research Academy, Powai, Mumbai 400076, India; and Indian Institute of Technology Bombay, Department of Metallurgical Engineering and Materials Science, Powai, Mumbai 400076, India
Talal Al-Samman: Institut für Metallkunde und Metallphysik, RWTH Aachen University, Kopernikusstr. 14, Aachen, 52074 Germany
Berengere J.C. Luthringer and Regine Willumeit: Helmholtz-Zentrum Geesthacht (HZG), Institute of Metallic Biomaterials, Max-Planck-Strasse 1, D-21502 Geesthacht, Germany

Introduction

Research into new magnesium-based alloys, especially for implantology, is burgeoning, owing to their unique property of biodegradation in physiological environment and reasonable biocompatibility [1–4]. Among commercial Mg alloys, Mg-Al-Zn alloys (mainly AZ31 and AZ91), Mg-Zn-Zr alloys (e.g. ZK60) and Mg-Y-RE alloys (e.g. WE43) have been investigated in detail for their biocompatibility and biodegradation. The presence of Al in AZ and rare earths (RE) in WE alloy series is of some concern because of their toxicity to the human body. Aluminium is potentially responsible for Alzheimer's disease, whilst RE elements are known to be very difficult to excrete through the kidneys. In search of Mg alloys with more bio-compatible alloying elements, researchers moved their attention to Mg-Ca alloys [2, 4, 5]. Among them, a binary Mg-1Ca alloy showed promising properties for bioimplant applications, although the alloy suffers from poor formability and low strength [1]. Nene et al. [5] reported that Li addition to Mg-1Ca alloy enhanced the mechanical properties without compromising its bio-response [5–7]. The addition of Li further helped reducing the density of the alloy 1.55±0.09 g/cm^3, thereby making it superior to most of Mg alloys in terms of specific strength, whilst maintaining its biocompatiblity [6, 7].

The effect of the alloying elements on the bio-properties of Mg alloys is reasonably well established and

understood [8, 9]. However, the data on the effect of the microstructure of the alloys on the bio-properties for any specific composition are relatively scarce. Microstructure was reported to govern the corrosion behaviour of most of the Mg alloys and thus there is a possibility that the microstructure would affect their bio-response, as well [7–9]. The current work mainly focuses on generating different microstructures in the new ultralight Mg-4Li-1Ca (LX41) alloy by conventional processing, as well as by severe plastic deformation techniques. The microstructure effect on bio-properties is also studied with a view to establish a microstructure-cytocompatibility relation as a basis for further magnesium alloy development in the future.

Experimental

Samples of LX41 alloy 10 mm×10 mm in size in the as-cast, TSR and ECAP conditions were used for investigation of biodegradation behaviour in Earle's Balanced Salt Solution (EBSS). Details of TSR processing are given in [5] and the ECAP processing is shown in Table 1. Biodegradation tests were carried out in EBSS (Sigma-Aldrich Chemie GmbH, Germany) in an orbital shaking platform at 37 °C. The surface morphology after immersion was characterised by scanning electron microscopy (SEM), and the formation of corrosion products was analysed by Energy Dispersive Spectroscopy (EDS) and X-Ray Diffraction (XRD). Plasma Atomic Emission Spectroscopy (ICP-AES) was used to determine the concentration of Mg, Li and Ca ions in EBSS after 7 days of immersion.

Prior to cell culture tests, samples in the as-cast, TSR and TA30 conditions were sterilised ultrasonically for 20 min in 70% ethanol (Sigma-Aldrich Chemie GmbH, Munich, Germany), and then incubated overnight in cell specific complete medium. L929 cells were cultured in Dulbecco's Modified Eagle's Medium (DMEM) supplemented with 10% foetal bovine serum (FBS, Merck, Darmstadt, Germany), 1% penicillin, and 100 mg mL^{-1} streptomycin (Life Sciences, Karlsruhe, Germany) in an incubator under physiological conditions (5% CO_2, 20% O_2, 95% relative humidity, 37 °C). 50,000 cells in 50 µL medium were seeded on samples in 12-well plates and were allowed to adhere onto the surface for 30 min. Thereafter 3 mL of medium were added to each well.

Cell viability was assessed via Live/Dead Viability/Cytotoxicity Kit (Life Technologies, Darmstadt, Germany), a two-colour fluorescence assay. After removing the cell culture, medium samples were washed with phosphate buffer solution (PBS, 137 mM NaCl, 2.7 mM KCl, 4.3 mM Na_2HPO_4, 1.4 mM KH_2PO_4, all chemicals from Sigma-Aldrich Chemie GmbH, Munich, Germany). Then they were transferred to a new 12-well-plate and covered with the staining solution (2 µL Calcein AM and 5 µL ethidiumhomidimer-1 in 5 mL PBS) and incubated for 20 min. Subsequently, the staining solution was replaced by PBS and the samples were directly examined with a fluorescent microscope (Eclipse Ti-S, Nikon, Düsseldorf, Germany). Living cells can be detected by using the FITC-filter (Ex: 465–495 nm, Em: 515–555 nm, Mirror at 505 nm) as green areas, whereas dead cells can be identified by using the Texas Red-filter (Ex: 540–580 nm, Em: 600–660 nm, Mirror at 595 nm) as red areas. The overlaying image was merged by the microscope software.

After being washed in PBS, the samples were critical point dried prior to SEM evaluation (Auriga; Carl Zeiss, Jena, Germany). In brief, after a glutaraldehyde (Sigma-Aldrich Chemie GmbH, Munich, Germany) fixation step, the carriers were stained in osmium tetroxide (Sigma-Aldrich Chemie GmbH, Munich, Germany) prior to an alcoholic dehydration row. Subsequently, the samples were critical point dried in 2-propanol (Sigma-Aldrich Chemie GmbH, Munich, Germany) to preserve cell morphology for observation in a Leica EM CPD300 (Leica Mikrosysteme Vertrieb GmbH, Wetzlar, Germany). Cells on carriers were then visualised in the low voltage mode of charge contrast, by SEM (Auriga; Carl Zeiss, Jena, Germany) with a lens detector.

Results

Characterisation of surface morphology and product formation upon immersion test

Immersion tests for samples of LX41 alloy with different processing history were carried out as per the protocol given in Section 2. They were further characterised by EDS and SEM to determine the nature and the morphology of the products formed on the surface. Figure 1 (A–D) shows secondary electron images for samples in the as-cast, TSR, TA30, and ECAP conditions upon immersion in EBSS.

Table 1: Details of ECAP processing schedule.

Pass number	Temperature (°C)	Back Pressure (MPa)	Reasoning
1	250	No back pressure	Temperature is above the recrystallisation temperature and thus expected to result in dynamic recrystallisation.
2	210	4.8–5.5	Temperature is just above the recrystallisation temperature and is expected to cause further grain refinement in the second pass due to greater grain boundary area available [10].
3	190	4.8–5.5	Lower processing temperature is expected to produce additional grain refinement over that in the previous pass [10], also decreasing the propensity for grain coarsening.
4	160	4.8–5.5	

Irrespective of the processing conditions, the presence of tubular cracks on the surface as a result of degradation reactions can be established.

Figure 2 shows the results of EDS analysis of the reaction products formed on the surface of the material upon the immersion tests. It clearly demonstrates the formation of mainly two important compounds: bone-like hydroxyapatite and magnesium hydroxide. The presence of Ca and Mg peaks in the EDAX scans suggests that HA formed contains Mg and Ca ions. Formation of HA and $Mg(OH)_2$ was also supported by XRD scans (Figure 3). The observed variation in HA peak intensity confirmed that microstructure had an effect on HA formation. As-cast and TA30 alloys showed a sharper and more pronounced HA peak, whereas TSR and ECAP processed specimens exhibited broader and less intensive peaks associated with HA.

XRD results (Figure 3) also showed formation of metastable octa-calcium phosphate (OCP) on the surface along with that of Lithium hydroxide. There also appeared a variation in the peak intensity for $Mg(OH)_2$ in the course of the processing. This variation was most pronounced for the ECAP-processed sample. This strongest peak associated with $Mg(OH)_2$ suggests the formation of a thick layer of $Mg(OH)_2$ on the surface during an early stage of degradation. This is consistent with the lower pH value found for the ECAP-processed specimens after 3 days of immersion.

Variation of pH and release of ions as a function of the microstructure for LX41

Figure 4 (A, B) shows the variation in pH as a function of time (3 and 7 days) for LX41 alloy having different microstructures. The nature of the pH evolution is found to be highly dependent on microstructure of the alloy for a constant degradation time. Particularly, after 3 days of immersion (i.e. at an early stage of degradation), as-cast and ECAP alloys showed a rapid change in pH, whereas TSR and TA30 alloys exhibited the least pH levels. At the end of the immersion tests, as expected, the as-cast alloy showed the highest pH of 10.8, whilst TA30 and TMP alloys also possessed increased pH levels (10.3 and 9.7, respectively) as compared to those after the third day of immersion. This demonstrates that microstructure plays a very significant role in governing the pH variation and provides a further cue towards a relation between the biodegradation and microstructure for the Mg-Li-Ca system. The dependence of the amount of ions released during degradation on pH and thereby on microstructure is discussed in subsequent sections.

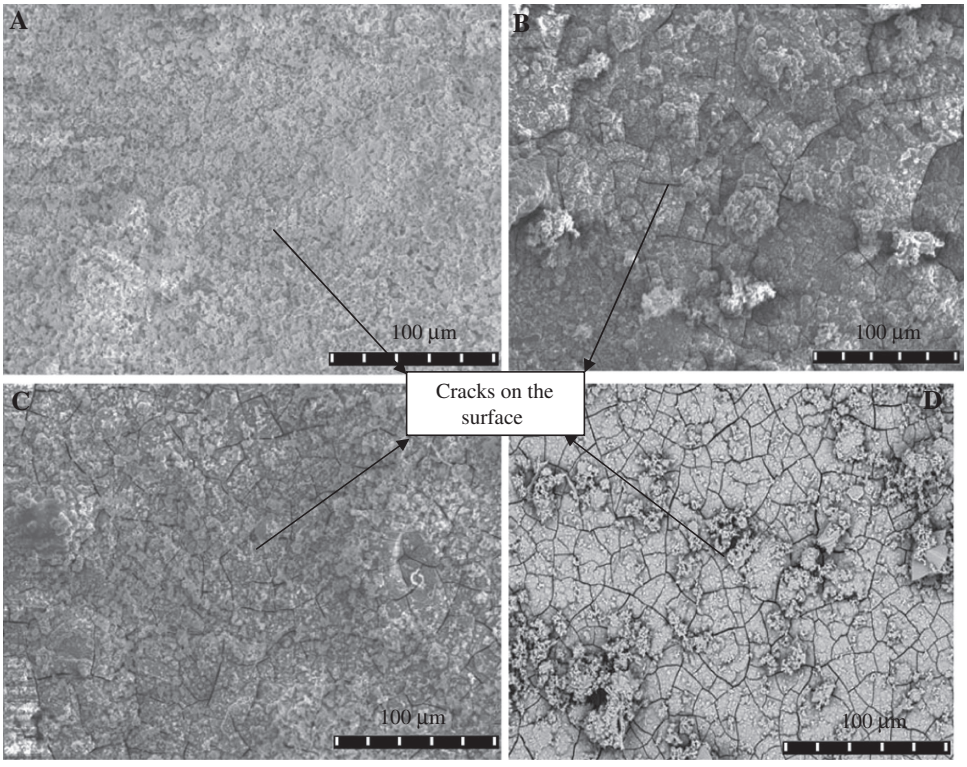

Figure 1: Secondary electron images showing surface morphology upon immersion in EBSS for 7 days for LX41 alloy in (A) as-cast, (B) TSR, (C) TA30, and (D) ECAP condition.

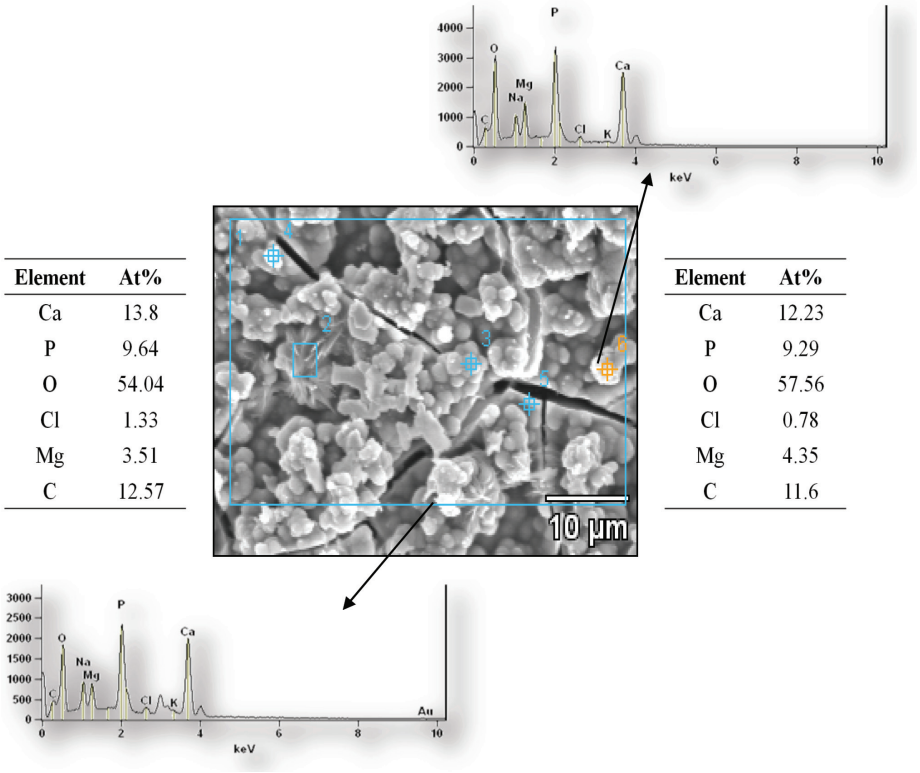

Element	At%
Ca	13.8
P	9.64
O	54.04
Cl	1.33
Mg	3.51
C	12.57

Element	At%
Ca	12.23
P	9.29
O	57.56
Cl	0.78
Mg	4.35
C	11.6

Figure 2: SEM and EDS analysis of LX41 alloy after 7 days in EBSS at 37 °C in an immersion test with an orbital shaking platform.

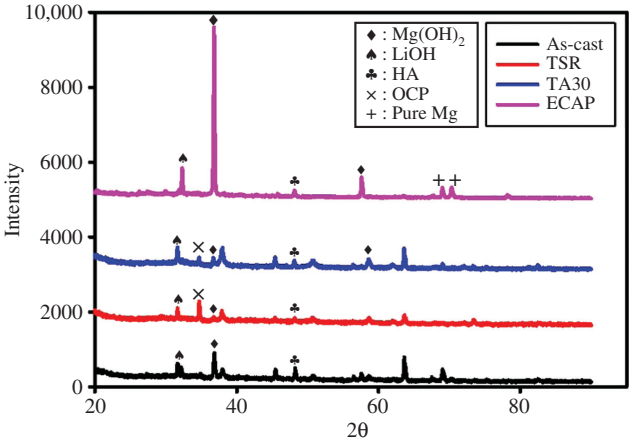

Figure 3: XRD patterns for LX41 alloy in four different conditions after immersion in EBSS at 37 °C (θ in degrees).

H_2 evolution

The pH level of the solution can be correlated with the hydrogen ion concentration. The amount of hydrogen evolved during the initial stage of degradation (after 3 days) was found to be the greatest, 2.237×10^{-3} mL/cm^2 and 2.220×10^{-3} mL/cm^2, for as-cast and ECAP alloys, respectively. These levels remained almost unchanged until the end of immersion, which is consistent with the early rise of pH for those alloys as described earlier. By contrast, TSR and TA30 alloys showed very low levels of H_2 evolution during the early stage of degradation, which substantially increased towards the seventh day of immersion, as seen in Figure 5 (A, B), following the same trend as for the pH variation.

Release of Li^{1+}, Mg^{2+} and Ca^{2+} ions

In order to estimate the magnitude of release for Li^{1+}, Mg^{2+}, and Ca^{2+} ions during degradation, ICP-AES experiments were carried out as mentioned in Experimental section. The ion release during degradation was found to be correlated with the pH variation. A plot of ion release vs pH obtained after the seventh day of immersion is given in Figure 6. It clearly shows that the Li ion concentration is the least for the TSR alloy, which exhibits a low pH of 9.8, whereas it is the highest (105 ppm) for the as-cast alloy, which exhibited a pH value of 10.6. The ECAP-processed alloy showed anomalous behaviour, with substantial levels of Mg^{2+} and Li^{1+} ions released into solution despite the lowest pH after 7 days of immersion.

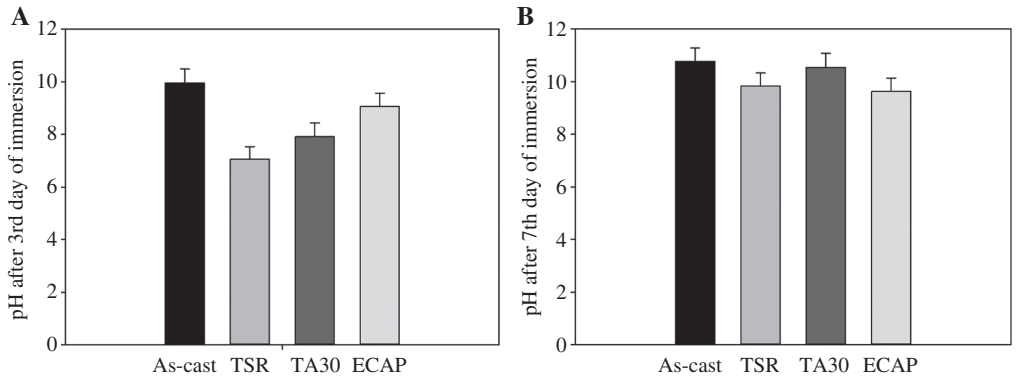

Figure 4: Dependence of pH on the microstructure after (A) three and (B) 7 days of immersion.

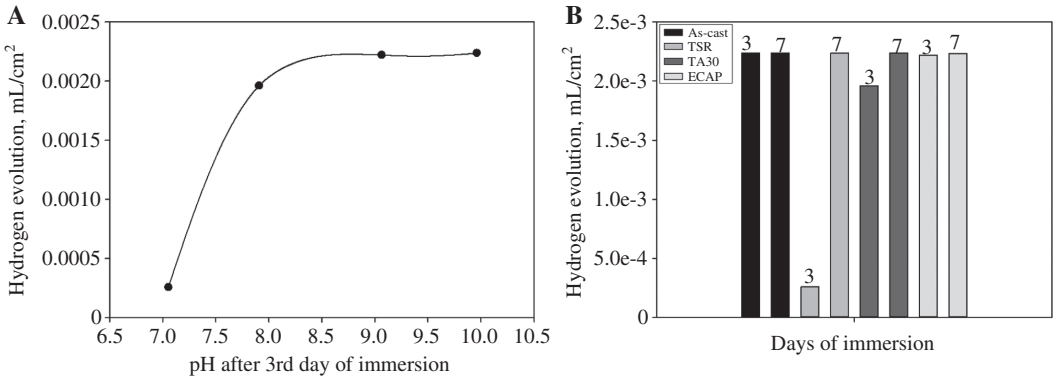

Figure 5: (A) hydrogen evolution vs. pH after 3 days of immersion, and (B) hydrogen evolution after 3 and 7 days of immersion for the various microstructural states of the alloy.

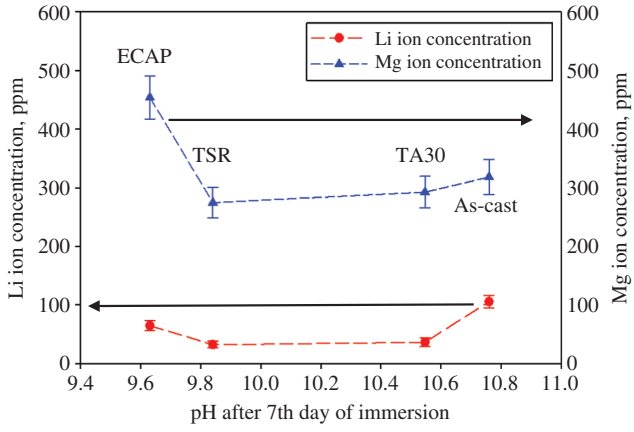

Figure 6: Li and Mg ion release as a function of pH after 7 days of immersion in EBSS for alloy LX41 with various processing histories.

However, a very rapid rise of pH to 9.06 in the early stage of degradation (3 days of immersion) for the ECAP alloy may have resulted in a higher level of released ions after 7 days of immersion.

Cytocompatibility evaluation for LX41 alloy

In order to investigate the cell response of the new LX41 alloy, cytocompatibility tests were carried out using L929 cells as mentioned in Experimental section. Figure 7 shows the live/dead staining results for the various microstructures after 7 days of incubation with 100% extract. The LX41 alloy exhibited cytocompatibility of more than 100% irrespective of the microstructure. However, among the alloys with the microstructures considered, the as-cast one showed a larger fraction of cells to appear live (green) than TSR alloy. TA30 alloy exhibited an intermediate number of live (green) cells upon incubation for 14 days in the alloy extraction medium with L929 cell culture (Figure 7). The morphology of L929 cells under SEM followed the same trend to support the happier and healthier cell morphology for as-cast and TA30 alloys than for TSR alloy after 14 days of culturing. Thus, the qualitative and quantitative measures of cytocompatibility, the cell morphology in SEM (Figure 8), and the character of the variation in the fraction of live cells during L929 cell culturing

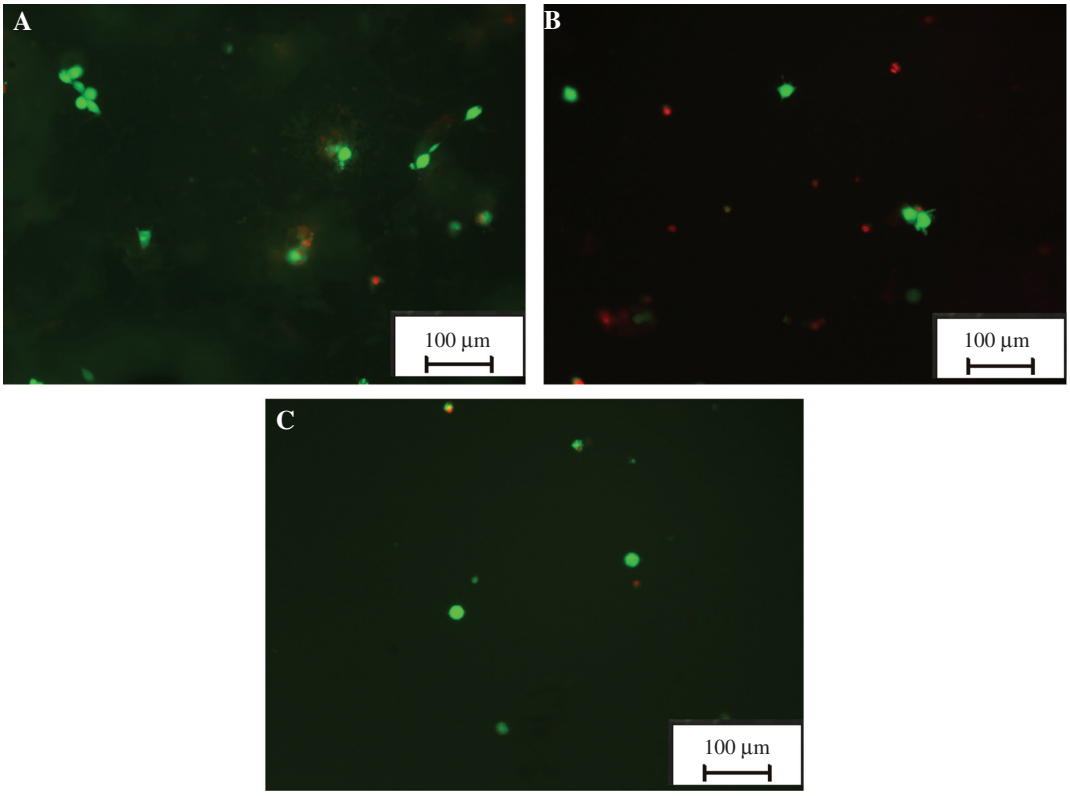

Figure 7: Live/dead staining results showing live (green) and dead (red) L929 cells after 14 days of incubation for (A) as-cast, (B) TSR, and (C) TA30 LX41 alloy.

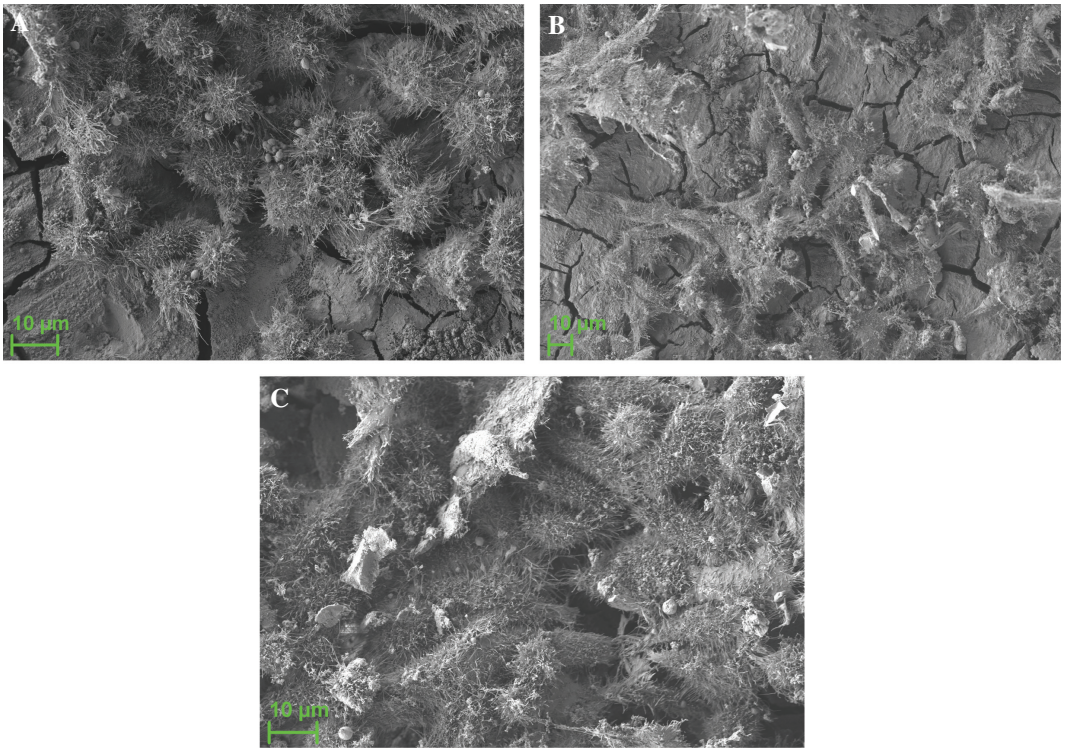

Figure 8: Secondary electron images showing L929 cell morphology after 14 days of incubation for LX41 alloy in (A) as-cast, (B) TSR, and (C) TA30 conditions.

provide evidence that the cell response has a direct connection with the microstructure of the alloy.

Discussion

Interrelationship between the pH variation and release of Li, Ca and Mg ions from LX41 alloy upon immersion in EBSS

Variation of pH during degradation is an important aspect for understanding the degradation mechanism. The rapid change in pH towards alkaline nature found for as-cast and ECAP alloys is associated with faster release of Mg ions into the solution, which further react with water and form a dense protective $Mg(OH)_2$ layer on the surface [1]. By contrast, a steady rise in pH for TSR alloy suggests a slower release of ions at the early stage of degradation, thereby forming a porous layer of $Mg(OH)_2$ on the surface. The TA30 material exhibited an intermediate level of release of Mg ions during degradation, thus forming a relatively dense layer of $Mg(OH)_2$ with a greater degree of corrosion protection than for TSR alloy. The rapid rise in pH for the as-cast alloy could be attributed to the more localised corrosion due to the presence of a very coarse grain structure containing continuous morphology of the eutectic in the as cast alloy. This was transformed to more uniform corrosion for the fine grained TSR alloy, where the eutectic particles were fragmented and distributed more uniformly leading to a steady rise in pH [1, 5–7].

While the release of Mg and Ca into the body fluid is not considered detrimental in terms of biotoxicity, that of Li may be regarded as having a concerning effect. A tolerable level of Li in the human body environment – before the pH level saturates to 10.5 during degradation – is below 75 ppm [6, 11]. In the present work, the Li level in EBSS was found to be affected by microstructure. It amounted to 36.2 and 32 ppm for TA30 and TSR alloys, respectively, for pH below the saturation levels of 10.5. This allays potential concerns with the use of the present alloy for medical implant applications, as the potential toxicity of Li can be kept at bay through appropriate engineering of the alloy's microstructure. Mg and Li ions released in the course of biodegradation get trapped within the hydroxyapatite layers formed at later stages of degradation and act as mediators between the cells and the substrate.

It was reported by Witte [2] that hydrogen release leads to formation of gas cavities during implantation of Mg in the human body, which is of great concern since it results in local swelling and pain to the patients. Therefore, this process needs to be inhibited. One recommendation that follows from the present work is to use alloy LX41 in the TA30 condition, for which the least amount of H_2 evolved in the early stage of degradation. We also note that the amount of hydrogen released was found to be very low compared to those reported for H_2 evolution by Li et al. [12] and Hofstetter et al. [13] for Mg-1.5Zn-0.6Zr-0.2Sc and Mg-5Zn-0.5Ca, respectively. It can be concluded that the composition and microstructure control can be used as an effective way to control the H_2 evolution.

Microstructure-biodegradation-cytocompatibility relationship for fine grained LX41 alloy

As-reported earlier, alloy LX41 undergoes corrosion in a particular fashion upon immersion in a physiological environment [6, 7]. During degradation by corrosion, Li, Ca, and Mg undergo anodic dissolution resulting in the formation of their respective ions. This is also accompanied with a cathodic reaction in which OH^- ions are formed and H_2 evolution takes place [1, 3, 4]. However, the presence of Mg_2Ca phase, which is more active than the constituent elements, results in the formation of local galvanic cells and thus promotes the corrosion reaction (Figure 9). The location and distribution of these active corrosion sites (the Mg_2Ca phase) is different for each microstructure and is associated with a specific mechanism of degradation [4, 7, 14–17]. As shown schematically in Figure 9 for TA30 alloy, with its equiaxed grain microstructure and a uniform distribution of active sites, degradation begins when the corrosion reaction is initiated by the Mg_2Ca phase. The uniform distribution of the corrosion sites ultimately leads to more homogeneous corrosion of the alloy along with the release of Li^{1+} and Mg^{2+} ions and H_2 gas [2, 6, 7]. Thus, the levels of the ion release are decided by the corrosion kinetics, i.e. ultimately by the microstructure inherited from the processing route used. These results provide the evidence of a strong microstructure-biodegradation relation, which can further be extended to the cytocompatibility response of the alloy considered.

Greater ion release by the as-cast alloy that corrodes faster and in a more localised way than the TSR material leads to higher pH in the kinetics of formation of OH^- ions (complementary cathodic reaction, [7]). That also means greater availability of OH^- ions for as-cast than TSR material that drives the corrosion reaction, Eq. (1), towards the formation of hydroxyapatite (HA). Similar considerations apply to TA30 vs. ECAP condition. Therefore, formation of HA is more favourable for the as-cast and TA30 alloys than

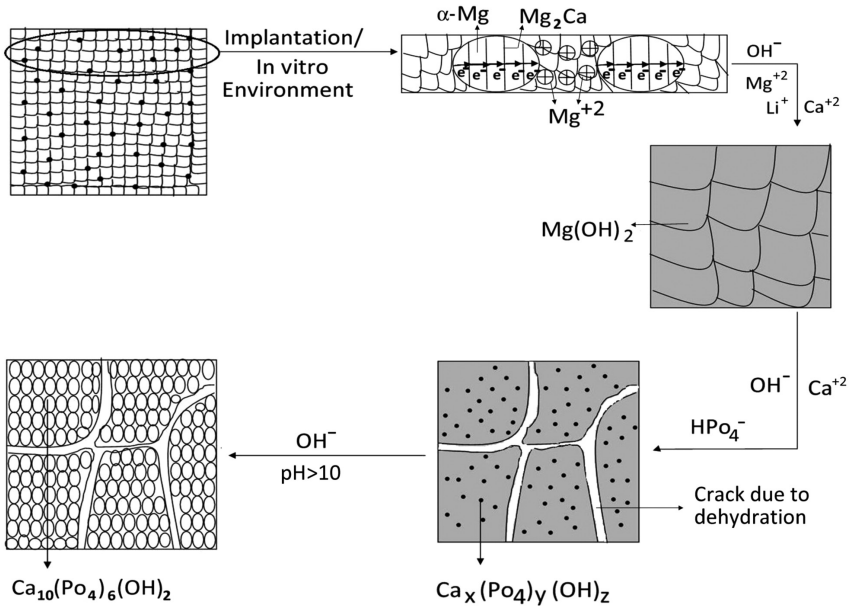

Figure 9: Schematic showing the mechanism of formation of a uniform layer of HA on the surface of LX41 during degradation (after [6]).

for TSR and ECAP alloys. During the formation of HA on the surface, part of Li^{1+} and Mg^{2+} ions get entrapped in it, as mentioned above.

$$xCa^{+2} + yPO_4^{-2} + zOH^- \rightarrow Ca_x(PO_4)_y(OH)_z \quad (1)$$

Once HA with entrapped Mg^{2+} and Li^{1+} ions is formed, these ions, as well as Ca^{2+} act as mediators between the cells and the alloy. In particular, Mg^{2+} and Ca^{2+} ions act as messengers in the interphase process of a cell cycle. Specifically, Ca^{2+} is of assistance in the G1 phase (increase in cell size by formation of proteins and m-RNA), whereas Mg^{2+} helps in accelerating the G1 to S phase transfer, thereby promoting cell growth. Li^{1+} also acts as a catalyst in the G1 phase to form proteins and m-RNA (provided its concentration is within the tolerance limit) [18, 19].

Thus, as understood from the above discussion, the formation of an HA layer with entrapped Mg^{2+} and Li^{1+} ions plays a key role in enhancing cell response and thus, indirectly, promoting cytocompatibility. As the formation of HA is a function of the amount of OH^- ions released, which is controlled by microstructure, there exists a strong microstructure-biodegradation-cytocompatibility relationship for LX41 alloy. As mentioned above, the effect of microstructure on the cytocomnpatibility of the alloy is illustrated in Figures 6 and 7. This microstructure-cytocompatibility correlation can potentially be extended to other degradable Mg alloys containing two galvanically coupled phases. It can be regarded as a possible tool in designing new bioresorbable Mg-based implants.

Conclusions

The present study of the effect of thermomechanical processing on the bio-response of ultralight LX41 alloy led to the following conclusions.

The properties of a magnesium based metallic system can be varied widely by composition design and thermomechanical processing. Specifically, the newly developed ultralight alloy of composition Mg-4Li-1Ca (LX41) was subjected to two step rolling process and ECAP. This resulted in an exceptionally high specific strength of LX41 alloy, which qualifies it for future use in lightweight structures.

In view of potential applications in biodegradable biomedical implants, the biocorrosion properties and cytocompatibility of LX41 in various microstructural states were investigated. The study revealed a significant favourable role of microstructure refinement by two-step rolling in terms of strength enhancement and biocorrosion resistance. The presence of Li in the alloy was shown not to translate to excessively high levels of Li ions in the solution. It was suggested that Mg, Li, and Ca ions entrapped in a hydroxyapatite layer formed on the alloy surface in body fluid, act as mediators between L929 cells and the LX41 substrate, thus promoting the formation of hydroxyapatite that inhibits biocorrosion.

Acknowledgments: The authors would like to thank Mr. Ajay Suryavanshi and Prof. R. Srivastava, Department of Bioscience and Bioengineering, IIT Bombay, for their

advice and support with biodegradation studies. Funding from the Department of Science and Technology, India, under FIST program SR/FST/ETII–054/2000 is acknowledged. YE would also like to acknowledge support from the Russian Ministry for Education and Science (grant #14.A12.31.0001) and the Helmholtz Association (Helmholtz International Fellow Award).

References

1. Li Z, Gu X, Lou S, Zheng Y. The development of binary Mg-Ca alloys for use as biodegradable materials within bone. Biomaterials. 2008;29:1329–44.
2. Witte F. The history of biodegradable magnesium implants: a review. Acta Biomater. 2010;6:1680–92.
3. Song GS, Kral MV. Characterization of cast Mg–Li–Ca alloys. Mater Charact. 2005;54:279–86.
4. Zeng RC, Sun L, Zheng YF, Cui HZ, Han EH. Corrosion and characterization of dual phase Mg-Li-Ca alloy in Hank's solution: the influence of microstructural features. Corr Sci. 2014;79:69–82.
5. Nene SS, Kashyap BP, Prabhu N, Estrin Y, Al-Samman T, Luthringer BJ, et al. Introducing an ultralight, high strength, biodegradable Mg-4Li-1Ca alloy. Adv Biomater Dev Med. 2015;1:32–6.
6. Nene SS, Kashyap BP, Prabhu N, Estrin Y, Al-Samman T. Microstructure refinement and its effect on specific strength and bio-corrosion resistance in ultralight Mg-4Li-1Ca (LC41) alloy by hot rolling. J Alloys Compd. 2014;615:501–6.
7. Nene SS, Kashyap BP, Prabhu N, Estrin Y, Al-Samman T. Biocorrosion and biodegradation behavior of ultralight Mg-4Li-1Ca (LC41) alloy in simulated body fluid for degradable implant applications. J Mater Sci. 2015;50:3041–50.
8. Gu X, Zheng W, Cheng Y, Zhong S, Xi T. In vitro corrosion and biocompatibility of binary magnesium alloys. Biomater. 2009;30:484–98.
9. Du H, Wei Z, Liu X, Zhang E. Effects of Zn on the microstructure, mechanical property and biocorrosion property of Mg-3Ca alloys for biomedical application. Mater Chem Phys. 2011;125:568–75.
10. Figueiredo RB, Langdon TG. Principles of grain refinement and superplastic flow in magnesium alloys processed by ECAP. Mater Sci Eng A. 2009;501:105–14.
11. Lu X, Leng Y. Theoretical analysis of calcium phosphate precipitation in simulated body fluid. Biomater. 2005;26:1097–108.
12. Li T, Zhang H, He Y, Wen N, Wang X. Microstructure, mechanical properties and in vitro degradation behavior of a novel biodegradable Mg-1.5Zn-0.6Zr-0.2Sc alloy. J Mater Sci Tech. 2015;31:744–50.
13. Hofstetter J, Martinelli E, Pogatscher S, Schmutz P, Povoden-Karadeniz E, Weinberg AM, et al. Influence of trace impurities on the in vitro and in vivo degradation of biodegradable Mg-5Zn-0.3Ca alloys. Acta Biomater. 2015;23:347–53.
14. Kirkland NT, Birbilis N, Walker J, Woodfield T, Dias GJ, Staiger MP. In-vitro dissolution of magnesium–calcium binary alloys: clarifying the unique role of calcium additions in bioresorbable magnesium implant alloys. J Biomed Mater Res Part B: App Biomater. 2010;95:91–100.
15. Jeong YS, Kim WJ. Enhancement of mechanical properties and corrosion resistance of Mg-Ca alloys through microstructural refinement by indirect extrusion. Corr Sci. 2014;82:392–403.
16. Song GL, Xu Z. Crystal orientation and electrochemical corrosion of polycrystalline Mg. Corr Sci. 2012;63:100–12.
17. Ralston KD, Birbilis N, Davies CH. Revealing the relationship between grain size and corrosion rate of metals, Scripta Mater. 2010;63:1201–4.
18. Hazelton B, Mitchell B, Tupper J. Calcium, magnesium and growth control in WI-38 human osteoblast cell. J Cell Bio. 1979;83:487–98.
19. Galli S, Naito Y, Karlsson J, He W, Miyamoto I, Xue Y, et al. Local release of magnesium from mesoporous TiO_2 coatings stimulates the peri-implant expression of osteogenic markers and improves osteoconductivity in vivo. Acta Biomater. 2014;10:5193–201.